Geotextiles and Geomembranes 31 (2012) 1–14

Contents lists available at SciVerse ScienceDirect

Geotextiles and Geomembranes

journal homepage: www.elsevier.com/locate/geotexmem

Sagging and filtration behaviour of nonwoven geotextiles overlying different bedding materials

Ennio M. Palmeira*, Janaina Tatto[1], Gregorio L.S. Araujo[2]

University of Brasilia, Department of Civil and Environmental Engineering, Faculty of Technology, 70910-900 Brasilia, DF, Brazil

ARTICLE INFO

Article history:
Received 30 April 2011
Received in revised form
13 August 2011
Accepted 18 September 2011
Available online 12 October 2011

Keywords:
Nonwoven Geotextile
Filter
Sagging
Bedding Material
Geotextile Strains

ABSTRACT

This paper presents and discusses the results obtained in laboratory tests to evaluate sagging and filtration behaviour of nonwoven geotextiles overlying particles of different bedding materials. Nonwoven geotextiles with masses per unit area of 200 g/m^2, 400 g/m^2 and 600 g/m^2 were used in the tests. Stainless steel spheres and gravels were employed as granular materials underlying the geotextile filter. Specific tests to evaluate the intensity of sagging of the geotextile filter in the voids of the underlying material were carried out. Average strains mobilised in the geotextile were assessed in the tests. The grain sizes of the particles that piped through the geotextile filter for different arrangements of spheres as bedding layer for the filter were measured. The results obtained showed that bedding conditions and geotextile structural characteristics can influence its retention capacity. Good comparisons between predicted and measured average geotextile strains were observed.

1. Introduction

Geotextiles have been extensively used as filters in drainage systems in geotechnical and geoenvironmental engineering works for the last decades. To function properly as a filter these materials must fulfil some requirements and several studies on geotextile filters can be found in the literature (Calhoun, 1972; Giroud, 1982, 1996, Carroll, 1983; Fannin et al. 1994; Lawson, 1986; Fischer et al. 1990; Bhatia and Huang, 1995; Lafleur, 1999; Palmeira and Fannin, 2002; Gardoni and Palmeira, 2002, for instance). Most of the filter criteria available were based on results from extensive laboratory testing programmes with different types of apparatus and with soil-geotextile filter systems being tested without the application of vertical stresses. Therefore, except under very low stresses, the current filter criteria do not reproduce accurately the conditions that a geotextile filter may find in the field. Besides other factors, stress level can influence the retention capacity and clogging conditions of the filter (Heerten, 1982; Faure et al. 1999; Gardoni and Palmeira, 2002; Palmeira and Fannin, 2002; Palmeira et al. 2005, 2010).

Another aspect yet to be properly investigated related to geotextile filter behaviour is the influence of the bedding conditions of the geotextile. In drains with gravel drainage material, the geotextile filter can sag in the pores of the gravel and the intensity of sagging is likely to influence its filter behaviour. For such drains, poor construction conditions or higher stress levels (Fig. 1a) increase the complexity of the problem, because of compression of the filter and more favourable conditions for mechanical damage, as shown in Fig. 1(b). For instance, Faure et al. (1999) reported small punctures in specimens of a geotextile filter exhumed from an embankment dam.

Sagging of the geotextile filter in the voids of the underlying coarse drainage material will also mobilise tensile stresses in the filter which, in addition to possible mechanical damage, may influence flow rate and filter retention capacities. Fourie and Kuchena (1995) investigated the behaviour of geotextiles specimens subjected to in-plane tensile stresses and verified that these stresses can have a marked effect on the flow rate capacity of the geotextile. Reductions of flow rates up to 80% were observed for woven and nonwoven geotextile specimens subjected to tensile loads smaller than 2.2% of the ultimate geotextile tensile strength. Fourie and Addis (1999) examined the variation of filtration opening sizes of two woven slit-film polypropylene geotextiles subjected to in-plane uni-axial and bi-axial stresses using

* Corresponding author. Tel.: +55 61 3107 0969; fax: +55 61 3273 4644.
E-mail addresses: palmeira@unb.br (E.M. Palmeira), janatatto@brturbo.com.br (J. Tatto), gregorio@unb.br (G.L.S. Araujo).
[1] Tel.: +55 61 3107 0958.
[2] Tel.: +55 61 3107 1272.

0266-1144/$ – see front matter © 2011 Elsevier Ltd. All rights reserved.
doi:10.1016/j.geotexmem.2011.09.002

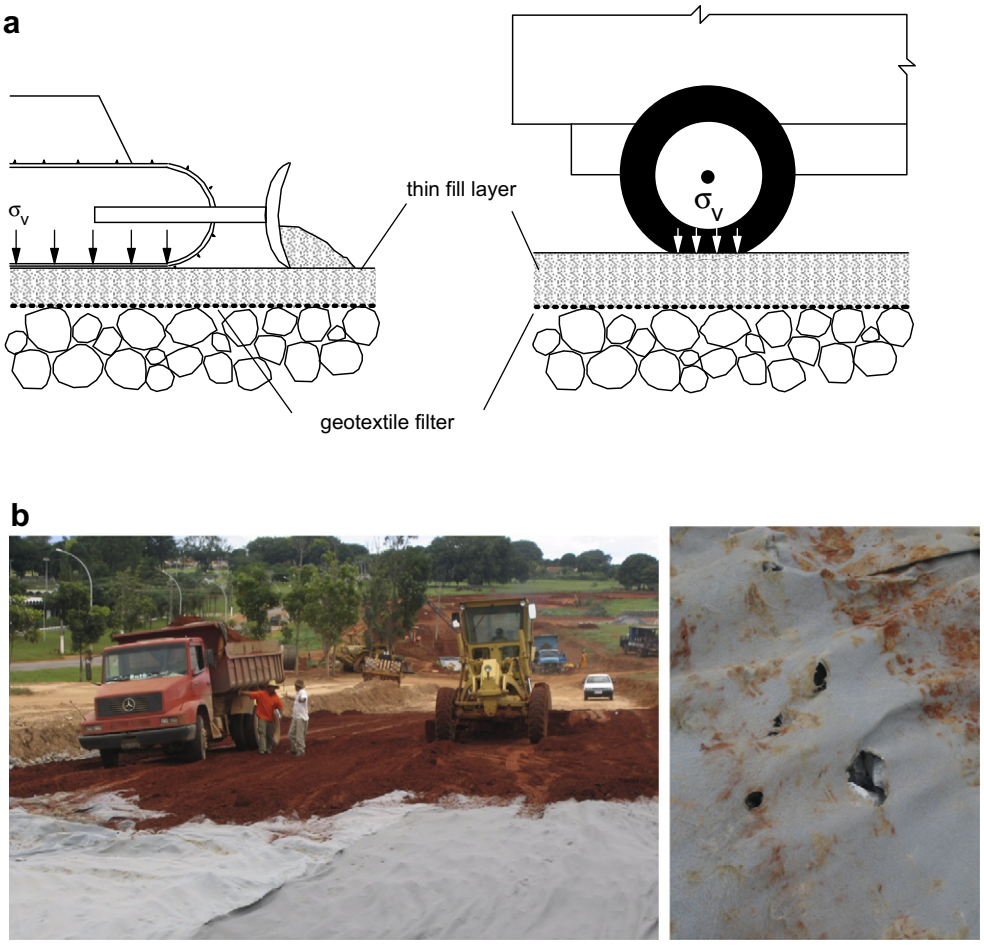

Fig. 1. Geotextile filters on coarse granular drainage layers. (a) Geotextile filter overstressing during construction, (b) Poor construction practice and filter damage.

a modified hydrodynamic sieving technique. The geotextiles were loaded up to about 10% of their minimum ultimate tensile strength and variations of filtration opening sizes of up to 28% were observed.

Wu et al. (2008) studied the influence of in-plane unidirectional tensile strain on the pore size and filtration characteristics of geotextiles. Heat bonded nonwoven and slit-film woven geotextiles were tested under tensile strains up to 20%. Tests to evaluate the apparent opening size (AOS) and the gradient ratio (Gradient Ratio Tests) were performed on stretched geotextile specimens without confinement (no vertical stresses on the specimens). The results of the experimental programme showed that the value of AOS increased and the value of gradient ratio decreased for the strained geotextile specimens in comparison with the unstrained ones.

Wu et al. (2006) performed gradient ratio tests on nonwoven geotextile filters overlying different bedding materials consisting of a perforated plate and steel spheres of varying diameters. The study focused on the variation of flow rate capacity and gradient ratio with the open area available for flow (total internal permeameter area minus geotextile-particle contact areas). The results obtained showed that the lower the open area in the underlying drainage material, the lower the values of flow rate capacity and gradient ratio.

This paper examines the influence of nonwoven geotextile sagging in the voids of different coarse granular materials under confinement on its retention capacity. The amount of sagging, average strains and retention capacity of the geotextile filter were assessed under more realistic conditions.

2. Experimentals

2.1. Equipment and methodology employed in the tests

The experiments carried out aimed at investigating the influence of the geotextile-bedding conditions on its filter behaviour. For that, a filtration apparatus similar to that used in Gradient Ratio Tests (Calhoun, 1972; Fannin et al. 1994; Palmeira et al. 1996) was employed after some modifications. Fig. 2(a) presents schematically the equipment used. The main changes made to the traditional GR test equipment were those necessary to accommodate the granular material underneath the geotextile filter and for that the original permeameter described by Gardoni (2000) had its lower cell increased in height. It is important to note that the measurement of the gradient ratio (GR) was not the objective of the research programme. The top cell of the permeameter confined the base soil overlying the geotextile. A loading platen allowed the application of normal stresses up to 2000 kPa on the soil-geotextile system. A load cell and a displacement transducer (LVDT) allowed the measurement of forces and displacements of the loading platen.

In the first part of the study the amount of geotextile sagging in the granular bedding material voids was assessed. Steel spheres and gravel particles were used as bedding materials with different values of spacing between individual particles. In these tests, after the application of a given normal stress on the base soil and stabilisation of displacement readings, the permeameter was carefully disassembled to allow the observation and measurements in the deformed geotextile layer. The deformed shape of the geotextile

layer at the end of a test was obtained using two different techniques. In the first one an extensible metallic foil (0.01 mm thick with a tensile stiffness of 10.2 kN/m from wide strip tensile tests) was installed underneath the geotextile layer, as shown in Fig. 2(b). In order to assess the influence of the stiffness of the foil and possible foil rebound after unloading on the results obtained, tests were also conducted with the use of layers of plaster and rubber foam underneath the geotextile layer, as schematically shown in Fig. 2(c). Both techniques yielded similar results. At the end of the test, digital photographs and micrometers readings were taken to obtain the geotextile deformed shape and sagging intensity in several points, respectively, based on the deformed shape of the metallic foil or of the plaster surface. Other relevant dimensions and contact areas between geotextile and bedding soil particles were also obtained from the digital photographs using an image processing software.

Two mechanisms to favour piping of soil particles through the geotextile filter were employed for the evaluation of the geotextile retention capacity. In the first one, the driving mechanism causing soil piping was water flow under a hydraulic gradient equal to 10, as in conventional filtration tests. The second mechanism employed tapping on the permeameter external walls using a rubber weight. A tapping device consisting of a rubber weight fixed to an arm was attached to the reaction frame of the permeameter cell to cause impacts on its walls under repetitive conditions. In each blow, the weight fell from a fixed height rotating like a pendulum to hit the permeameter cell. The impacts were uniformly distributed along the permeameter walls with a frequency of 0.33 Hz for 10 min. Each impact transferred to the system an amount of energy of 1.64 J. A similar procedure is described by Palmeira and Fannin (1998). Despite not being the actual mechanism causing soil particle piping in a filter in the field (although in some applications the filter may be subjected to vibrations), the piping triggering mechanism adopted can be considered as a conservative approach and allowed a quicker comparison among retention capacities of different geotextiles on the same basis. In both types of mechanisms causing soil particle piping the soil-geotextile system was tested under confinement, with the normal stress on the soil sample top being kept constant during the test.

The soil particles that piped through the geotextile filter were collected in the lower permeameter cell for grain size analysis. These analyses were conducted using a laser beam grain size analyser (Malvern Martersizer, UK). Microscopy analyses were also carried out as part of the investigation.

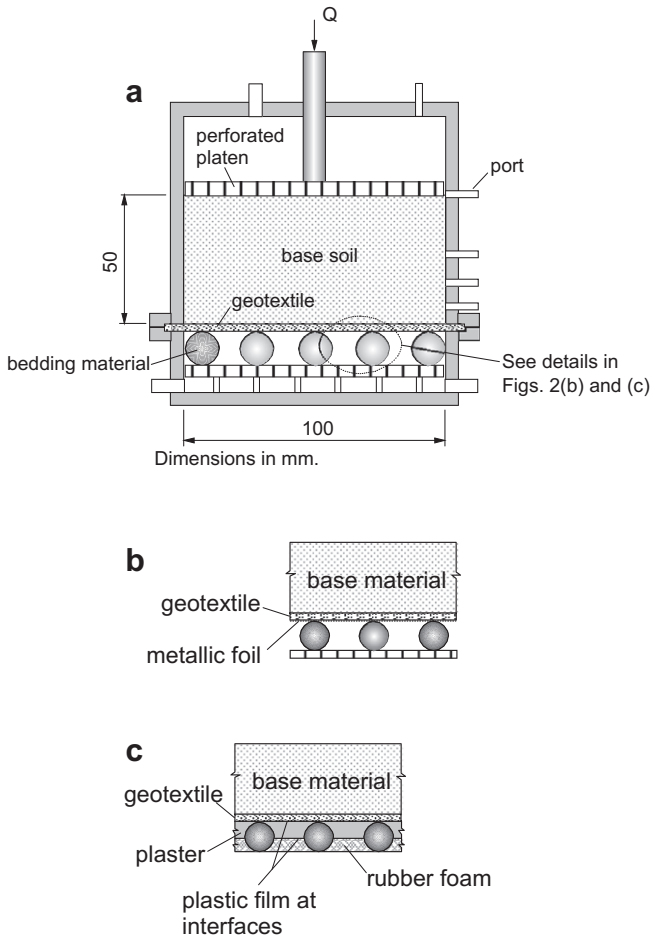

Fig. 2. Testing apparatus and bedding conditions. (a) Test equipment. (b) Geotextile overlying metallic foil. (c) Geotextile overlying plaster and foam.

2.2. Materials used in the tests

The base soil overlying the geotextile filter consisted of a mass of glass beads with 92.1% in mass of particles with diameters between 0.026 mm and 0.206 mm and a coefficient of uniformity equal to 1.6. The main properties of this material are summarised in Table 1. The glass beads would simulate closer a base soil consisting of round (spherical) particles, which would be a particular case. Less interlocking occurs among round particles in comparison with angular ones, which may favour an easier passage of the former through the geotextile. However, the results obtained using glass beads may be considered conservative on this regard and the uniformity and homogeneity of the glass beads bring several advantages regarding the interpretation of test results, better accuracy of grain size measurements and easier back-analyses of test results by current theoretical methods. In the tests aiming at determining the diameter of the maximum base soil particle capable of piping through the geotextile the base soil sample was prepared in a loose state (initial void ratio of 0.8) using the pluviation technique, as proposed by Vaid and Negussey (1988) for uniform materials. Loose soil samples were tested to minimise geotextile pore impregnation by base soil particles that would occur during base soil compaction, which would increase geotextile retention capacity and reduce particle piping through the geotextile filter.

The bedding granular material was simulated by stainless steel spheres and uniform gravel particles (cubical and triangular particle shapes). Two different particle diameters were used for each material. The diameters of the spheres used were equal to 10 mm and 18 mm. Gravel particles with approximately the same average diameters (10 mm and 19 mm) were selected by sieving. Gravel 1 and Gravel 2 had the same average particle diameter (10 mm) but different particle shapes, as shown in Fig. 3(a). The shape of the particles of Gravel 1 was predominantly triangular,

Table 1
Properties of the base soil (glass beads).

Percentage[a] of particles with D > 0.206 mm (%)	6
Percentage of particles with 0.026 mm < D ≤ 0.206 mm (%)	92.1
Percentage of particles with D < 0.026 mm (%)	1.9
Density (Mg/m^3)	2.5
D_{50} (mm)	0.126
D_{10} (mm)	0.086
CU	1.6
Minimum particle compressive strength (MPa)	97

D = particle diameter, D_n diameter for which n % of the remaining particles have diameters smaller than that value, CU = coefficient of uniformity (= D_{60}/D_{10}).
[a] in mass.

whereas that of Gravel 2 was predominantly cubical. Gravel 3 (19 mm average particle diameter) had both cubical and triangular particles (Fig. 3b). The gravels used had high sphericity, according to the classification proposed by Powers (1953). Thus, materials with similar grain sizes and grain size distribution curves but different particle shapes were employed to assess the influence of the bedding soil particle shape on the test results.

Fig. 4(a) presents the relevant dimensions of the pack of particles used throughout this work, whereas Fig. 4(b) shows how the average geotextile tensile strain was estimated based on the measurements taken during the tests. The particles of the bedding material were distributed in the lower permeameter cell in a triangular pattern with ratios between spacing between particles (s = centre to centre distance, Fig. 4(a)) and particle diameter (d) varying between 1 (densest arrangement, with particles in direct contact) and 2 (loosest arrangement tested).

Three nonwoven, needle-punched, geotextiles made of continuous filaments of polyester were employed in the tests. Table 2 presents relevant information on the geotextiles tested. The mass per unit area of the geotextiles varied between 200 g/m^2 (geotextile G1) and 600 g/m^2 (geotextile G3) and their filtration opening sizes between 0.06 mm (geotextile G3) and 0.14 mm (geotextile G1), according to manufacturer's catalogue data.

3. Results obtained

3.1. Geotextile sagging in the voids of the bedding material

3.1.1. Tests with spheres as bedding material

Fig. 5(a) and (b) show the variation of average maximum geotextile sag (δ_{max} in Fig. 4) with vertical stresses on the base soil top for tests on geotextile G1 with bedding material consisting of spheres with diameters of 10 mm and 18 mm, respectively. It can be noted that, in most cases, most of the sagging takes place for normal stresses up to 50 kPa. For vertical stresses greater than 200 kPa on the base soil sample top and for the smallest sphere diameter (Fig.5a) geotextile sagging increased at a greater rate for values of s greater than 13.3 mm ($s/d > 1.33$). For the largest sphere diameter (Fig. 5(b)) and larger distances between spheres ($s = 30$ mm and $s = 36$ mm) significant sagging of the geotextile in

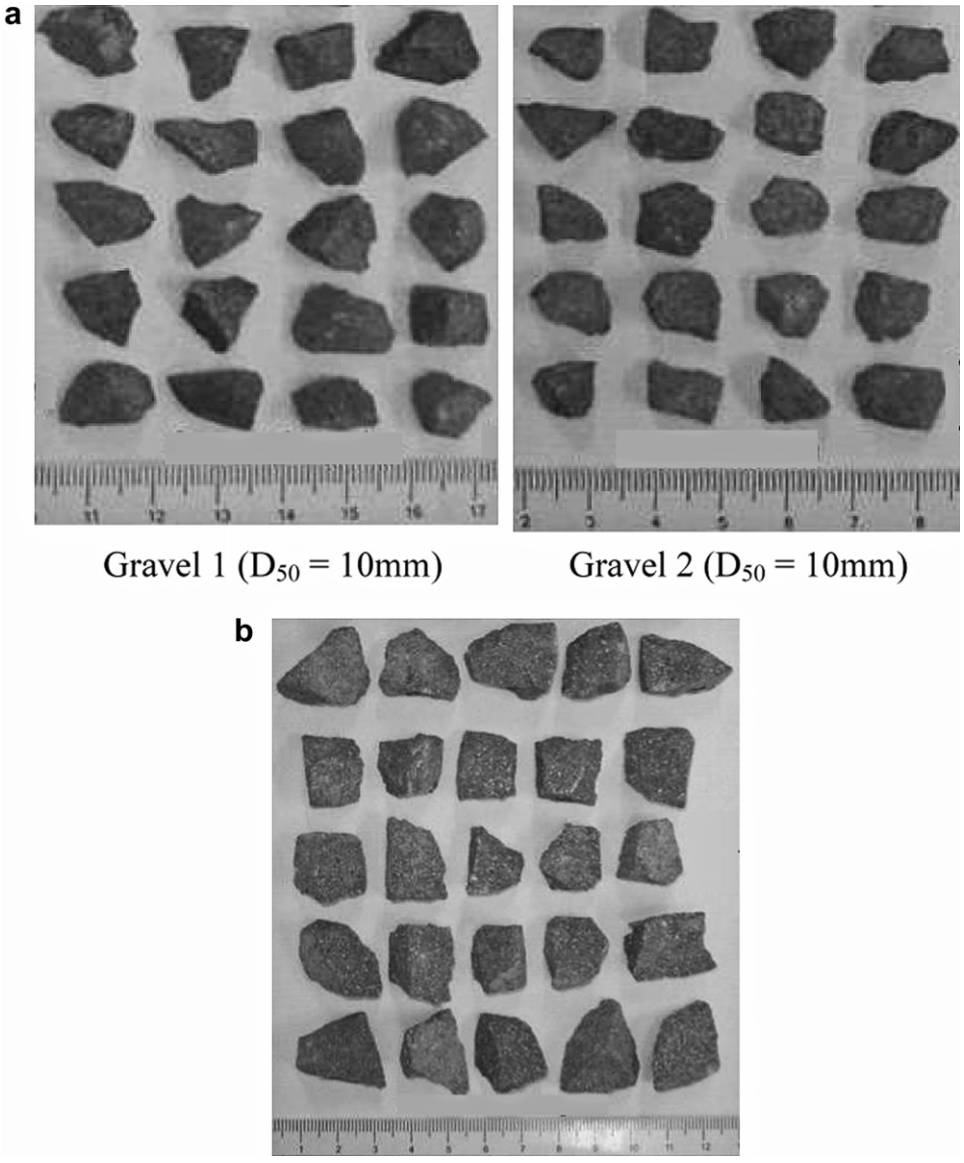

Fig. 3. Particles of materials used in the tests. Gravel 1 (D_{50} = 10 mm) Gravel 2 (D_{50} = 10 mm), (b) Gravel 3 (D_{50} = 19 mm).

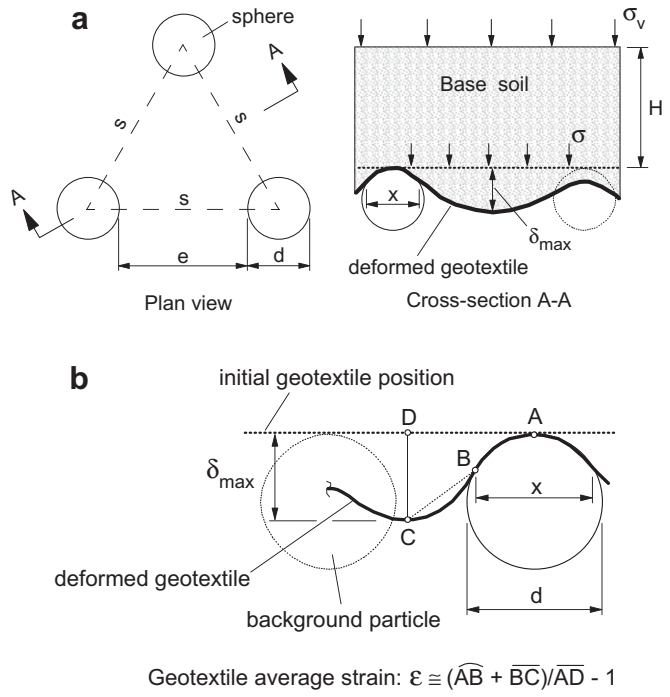

Fig. 4. Relevant dimensions at the geotextile-bedding material interface. (a) Relevant dimensions of the pack of particles. (b) Estimate of average geotextile tensile strain.

the voids of the underlying material can be observed, particularly for stresses greater than 500 kPa, which also raises concerns on the possibility of geotextile damage in the field under similar conditions, as will be discussed later in this paper.

One should note that the vertical stress on the void between the particles of the bedding material can be significantly smaller than that applied on the top of the base soil because of soil arching. Among other factors, the vertical stress on the void depends on the value of *s*. This stress can be estimated based on the solution proposed by Giroud et al. (1990), as will be discussed later in this paper. For the conditions used in the tests the vertical stress on the voids varied between 0.8 kPa (for $d = 10$ mm and $s/d = 1$) and 601 kPa (for $d = 18$ mm and $s/d = 2$) according to Giroud et al. (1990).

Fig. 6(a) to (c) present images of the shape of the metallic foil underneath the geotextile layer at the end of tests on geotextiles G1 and G3 under different normal stresses and bedding conditions. It can be observed the complex three dimensional shape assumed by the geotextile filter depending on the stress level and on the diameter and distance between the particles of the bedding material. Wrinkles in the metallic foil can be noticed along the sphere centre to centre directions, which would suggest that light geotextile filter layers would be prone to wrinkle along these directions. This is also corroborated by the image in Fig. 7(a), which shows the shape of the contact surface between plaster and geotextile G1 at the end of a test under 200 kPa. In this case, plaster was used as base material, as well as underneath the geotextile (Fig. 2c), to assess geotextile sagging, rather than the metallic foil. The impressions left by the spheres, the regions of maximum sag and the wrinkles mentioned above can be clearly seen. However, under large stress levels and large values of s/d these wrinkles may not be present, as it is suggested by the image in Fig. 7(b), which shows the deformed shape of geotextile G1 tested on 18 mm diameter spheres, with $s = 36$ mm ($= 2d$) under 2000 kPa normal stress. The bright spots in this image are of particular relevance, as they are the deformed shapes of holes left by the needles after the needle-punching geotextile manufacturing process. As it will be seen later in this paper, these holes may have a significant influence on

Table 2
Geotextile properties.

Code	M_A (g/m^2)	t_{GT} (mm)	FOS (mm)	k_n (m/s)	ψ (s^{-1})	n (%)	T_{max} (kN/m)	ε_{max} (%)
G1	200	2.9	0.14	2.2×10^{-3}	0.76	93	15	50–65
G2	400	3.8	0.09	2.2×10^{-3}	0.57	92	29	50–65
G3	600	5.9	0.06	2.2×10^{-3}	0.37	91	38	50–65

Notes: Data from manufacturer's catalogue; M_A = geotextile mass per unit area; t_{GT} = geotextile thickness; FOS = geotextile filtration opening size (= O_{95} = opening size for which 95% of the remaining openings are smaller than that value) from hydrodynamic tests (CFGG, 1986); k_n = cross-plane geotextile permeability coefficient; ψ = geotextile permittivity; n = geotextile porosity; T_{max} = tensile strength (wide strip tests, CFGG, 1986); ε_{max} = maximum geotextile strain (wide strip tests, CFGG, 1986).

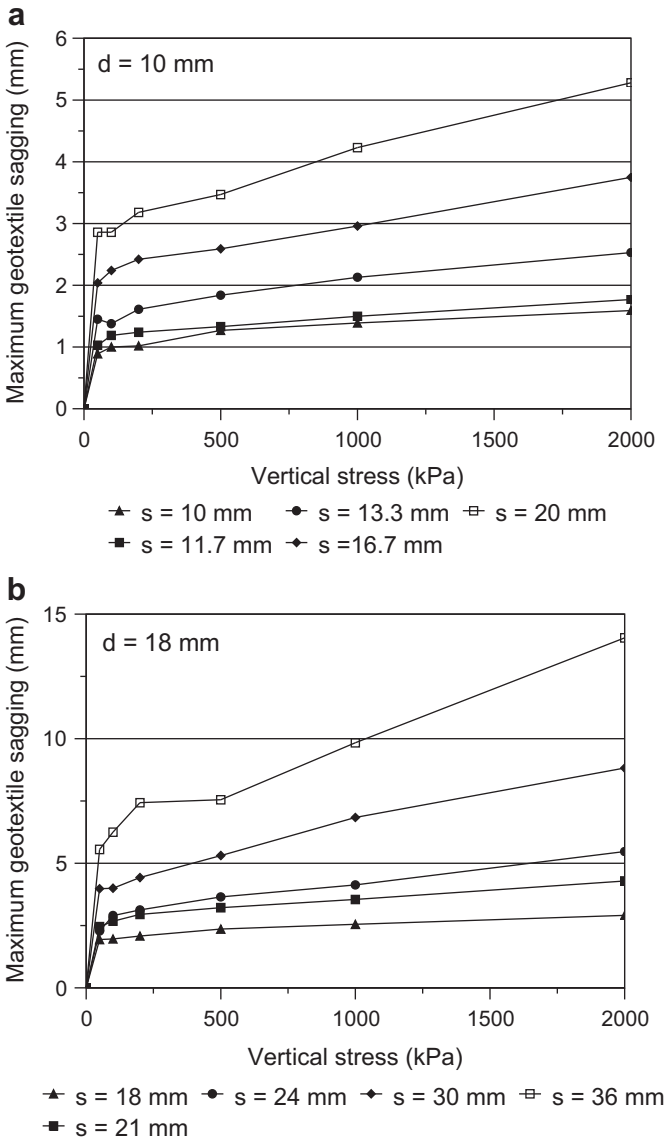

Fig. 5. Maximum geotextile sagging versus vertical stress – Tests with spheres and G1. (a) $d = 10$ mm (b) $d = 18$ mm.

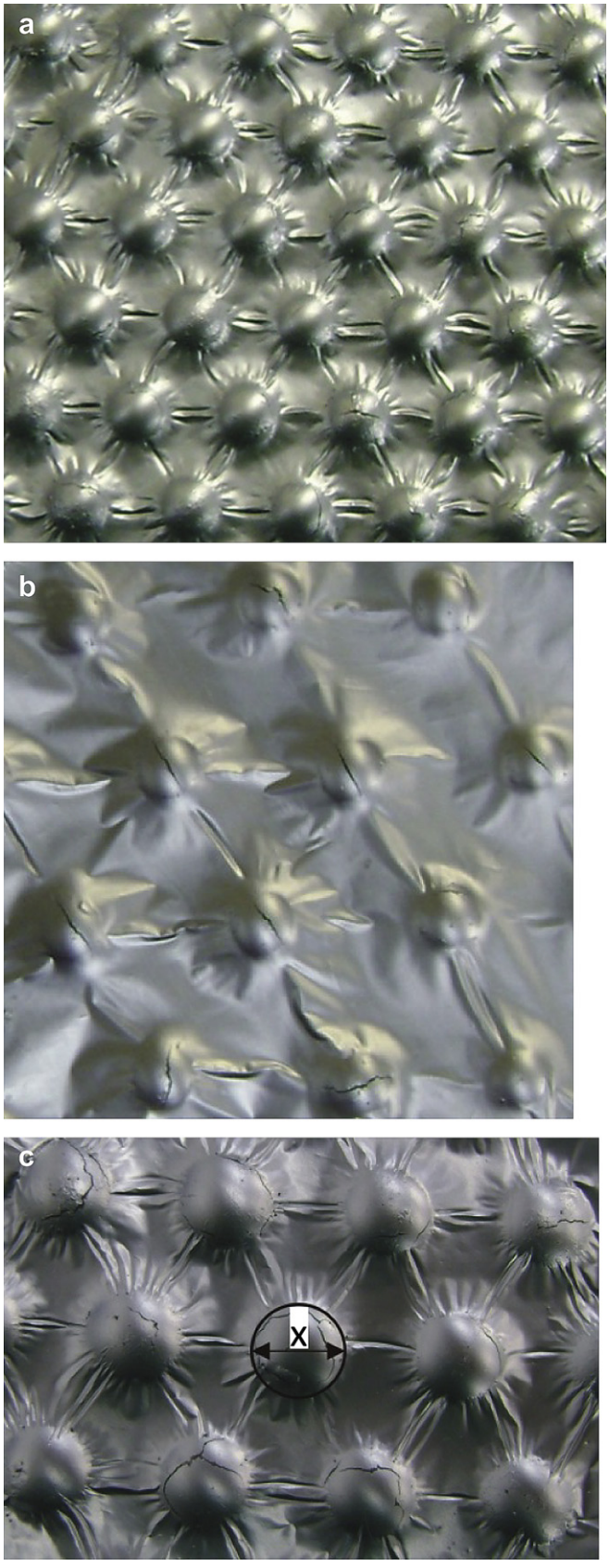

Fig. 6. Images of the deformed shape of the metallic foil underneath the geotextile. (a) Geotextile G1, d = 10 mm, s/d = 1, 1000 kPa vertical stress. (b) Geotextile G3, d = 18 mm, s/d = 1.17, 50 kPa vertical stress. (c) Geotextile G1, d = 18 mm, s/d = 1, 1000 kPa vertical stress.

the diameter of the base soil particle capable of passing through the geotextile. Signs of geotextile tearing at its contact with the sphere can also be noted in Fig. 7(b).

The analysis of the deformed shape of the metallic foil also allowed assessing the diameter (x in Fig. 4b) of the contact area between the deformed geotextile layer and the spheres. Fig. 8(a) and (b) show the variation of the contact diameter (x) normalised by the sphere diameter (d) with the vertical stress for geotextile G1 under different bedding conditions. It can be observed that x/d increases at a greater rate up to a vertical stress of 50 kPa on the base soil sample top. In most cases the rate of increase of x/d with vertical stress is significantly smaller for vertical stresses greater than 500 kPa. The value of x/d tend to become constant after 1000 kPa vertical stress for the tests with the smallest sphere (d = 10 mm, Fig. 8a). However, that was not the case for the tests with the largest sphere (Fig. 8b). For the largest value of sphere diameter (d = 18 mm) and largest spacing (s) between spheres the value of x/d was close to unity for a vertical stress of 2000 kPa (see also Fig. 7b). This can be explained by the larger void volumes between large particles, which allow greater sagging of the geotextile. These larger voids also favour larger amounts of base soil particles to push the geotextile downwards, as the arching mechanism in between the bedding material particles is reduced.

The influence of geotextile mass per unit area on geotextile sagging can be seen in Fig. 9(a) in terms of maximum geotextile sagging (δ_{max}) versus normalised spacing between spheres (s/d) for vertical stresses on the base soil sample of 50 kPa and 1000 kPa. In general, the larger the geotextile mass per unit area the smaller its maximum sagging. Not much influence of the mass per unit area can be observed for values of s/d up to 1.2. The influence of mass per unit area becomes more significant for a value of s/d equal to 2. Similar conclusions can be drawn regarding the influence of the mass per unit are on the diameter of the contact area between geotextile and spheres, as shown in Fig. 9(b).

3.1.2. Tests with gravel particles as bedding material

Tests were also conducted using gravel materials in order to assess geotextile sagging under more realistic conditions. The gravel materials tested were selected in terms of grain sizes and shape to allow comparisons with the results of tests where spheres were employed. This allowed assessing the influence of bedding particles shape on sagging intensity. In these tests the gravel particles were arranged in direct contact among them, as in the tests with spheres for s/d = 1 or e = 0 (Fig. 4a). Fig. 10(a) and (b) show views of the arrangements of gravel particles in some of the tests performed.

Fig. 11(a) shows comparisons between values of average maximum geotextile sagging in voids between sphere and gravel particles for tests with geotextile G1, 10 mm particle diameter and s/d = 1, under 500 kPa normal stress. The results show that sagging was more intense in case of gravel bedding material, with the average value of maximum sagging under these conditions being of the order of two times that observed for the spheres. Fig. 11(b) presents similar results for tests with geotextile G1 under 500 kPa, with 19 mm diameter gravel particles and 18 mm diameter spheres as bedding materials. In this case, the intensity of sagging in the test with the 19 mm diameter gravel particles was approximately 36% greater than that with spheres.

It should be pointed out that although the results of the tests with spheres shown in Fig. 11 were those with s/d = 1 and that the gravel particles were in direct contact, the non uniform shape of the gravel particles makes impossible to avoid regions with values of s/d greater than one (Fig. 10). This fact and the lack of symmetry of the gravel particles yield that in the tests with gravel particles there are regions were the values of s ($= e + d$) are larger than that

obtained with a regular pack of spheres, despite the gravel particles and spheres having approximately the same diameter. Measurements of s in tests with particles of Gravels 1 to 3 in direct contact yielded the results presented in Table 3, where it can be noted maximum values of s between 77% and 144% greater than the gravel particle diameter, whereas in the pack of spheres that value would be equal to the sphere diameter. Thus, one cannot make direct comparisons between results of tests with gravel and spherical particles with the same diameter and a similar particle arrangement.

Because the value of s is not uniform in a pack of gravel particles assembled aiming at having $s/d = 1$, a more reasonable comparison between results of tests with spheres and gravel particles seems to be in terms of average values of s for the gravel particle arrangement. Fig. 12 shows normalised maximum geotextile sagging in between particles (δ_{max}/d) versus s/d (average values of s for the tests with gravels assembled aiming at $s/d = 1$) in tests with geotextile G1 under 500 kPa. This figure also shows the result obtained for the same geotextile and Gravel 3 for s/d = 2. The results for the tests with gravel are presented in terms of δ_{max}/d plus and minus one standard deviation and the figure also presents the results of tests with spheres for comparisons. Fig. 12 shows that in terms of similar average values of s the average maximum normalised geotextile sagging (δ_{max}/d) in a pack of gravel particles can be considerably larger than that in a pack of spheres (up to 71% greater in the pack of gravel particles). The results obtained for Gravel 3 (larger particles) were rather close to those obtained for the sphere with similar diameter for both $s(average)/d$ equal to 1 and 2.

The region where maximum sagging occurs at the geotextile filter-bedding material interface is likely to be the most critical one regarding filter retention capacity due to high levels of geotextile tensile strains and more favourable conditions for filter perforation by neighbour gravel particles. It should be pointed out that at this stage the results reported in this paper should not be generally extrapolated to other gravel bedding conditions. Obviously, bedding conditions involving the use of more rounded particles are likely to be better simulated by a pack of spheres with the same diameter and particle arrangement.

3.2. Average geotextile strains

Fig. 13(a) and (b) show the variation of the average geotextile tensile strain (see Fig. 4(b)) with normal stress on the base soil top for tests with geotextile G1, spheres with 10 mm and 18 mm diameter and varying values of s/d. It can be seen that in most cases the strain increased with normal stress at a greater rate for normal stresses below 50 kPa. The lower the s/d ratios, the greater the capacity of soil arching above the bedding material voids to limit the strains mobilized in the geotextile. A clear change in the rate of mobilized geotextile strain with normal stress can be noted in the test with the largest sphere diameter ($d = 18$ mm) and s/d equal to 2 at 500 kPa normal stress on the base soil sample top. In this test, for a normal stress of 2000 kPa, the tensile strain reached a value of the order of 52% of the average ultimate strain obtained in tensile tests (Table 2). Thus, under such conditions, damage of the geotextile may compromise its filter behaviour, particularly in the case of sharp gravel particles underlying the geotextile filter (note signs of geotextile tearing at the geotextile-sphere contact in Fig. 7(b) in the test with $d = 18$ mm, $s/d = 2$, G1, under 2000 kPa).

The influence of the geotextile mass per unit area (M_A) on the mobilized average geotextile strain can be seen in Fig. 14(a) to (c), where the results of average strains versus normalised spacing between spheres (s/d) obtained for geotextiles G1 ($M_A = 200$ g/m^2), G2 ($M_A = 400$ g/m^2) and G3 ($M_A = 600$ g/m^2) are depicted. Under a vertical stress of 1000 kPa, it can be noted the little influence of

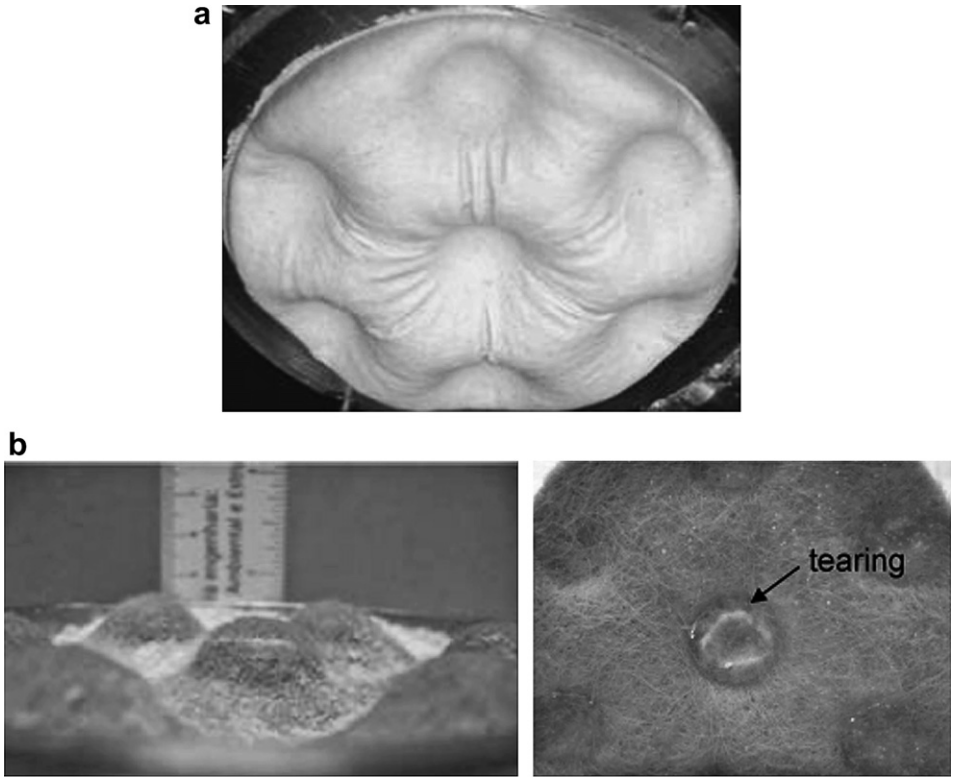

Fig. 7. Shape of geotextile surface – Geotextile G1. (a) Plaster-geotextile contact surface (vertical stress of 200 kPa). (b) Deformed geotextile (vertical stress of 2000 kPa).

the geotextile mass per unit area in the tests with the smallest spheres ($d = 10$ mm). That is a consequence of the smaller void volumes and openings between these spheres. The geotextile thickness certainly plays an important role in this case as well, as the smaller the openings between particles and the thicker the geotextile, the smaller the geotextile strain needed for it to occupy a significant fraction of the void volume in between particles. For the tests with 18 mm diameter spheres under 1000 kPa vertical stress the strains were smaller for the heavier geotextiles, but not inversely proportional to the increase in mass per unit area (Fig. 14(b)). Little difference between the results for geotextiles G2 and G3 can be observed in Fig. 14(b). For a lower vertical stress (50 kPa), d equal to 18 mm and values of s/d equal to 1.17 and 2, the results in Fig. 14(c) also show smaller strains in heavier geotextiles, as well as small differences between the average strains in geotextiles G2 and G3. The results in Fig. 14 suggest that for the materials and conditions employed in the tests a geotextile mass per unit area less than 400 g/m^2 would favour the development of larger geotextile strains.

3.3. Predicted versus observed average geotextile strains

It is interesting to investigate if the equations proposed by Giroud et al. (1990) for the estimate of average strains in geotextile layers overlying circular voids would be applicable to the conditions of the present tests. According to those authors, the average geotextile strain can be estimated by

$$\varepsilon = 2\Omega \sin^{-1}\left[\frac{1}{2\Omega}\right] - 1 \quad (\text{for} \delta/b \le 0.5) \tag{1}$$

or

$$\varepsilon = 2\Omega\left\{\pi - \sin^{-1}\left[\frac{1}{2\Omega}\right]\right\} - 1 \quad (\text{for} \delta/b \ge 0.5) \tag{2}$$

With

$$\Omega = 0.25\left(\frac{2\delta}{b} + \frac{b}{2\delta}\right) \tag{3}$$

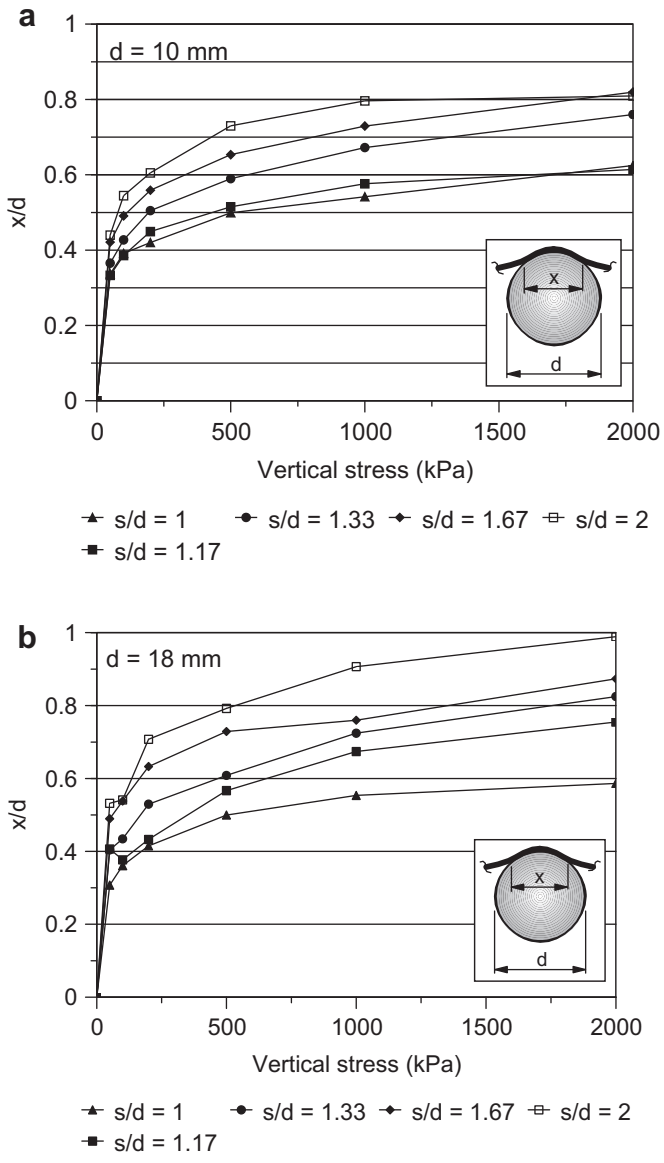

Fig. 8. Diameter of the contact area between geotextile G1 and sphere versus vertical stress. (a) $d = 10$ mm (b) $d = 18$ mm.

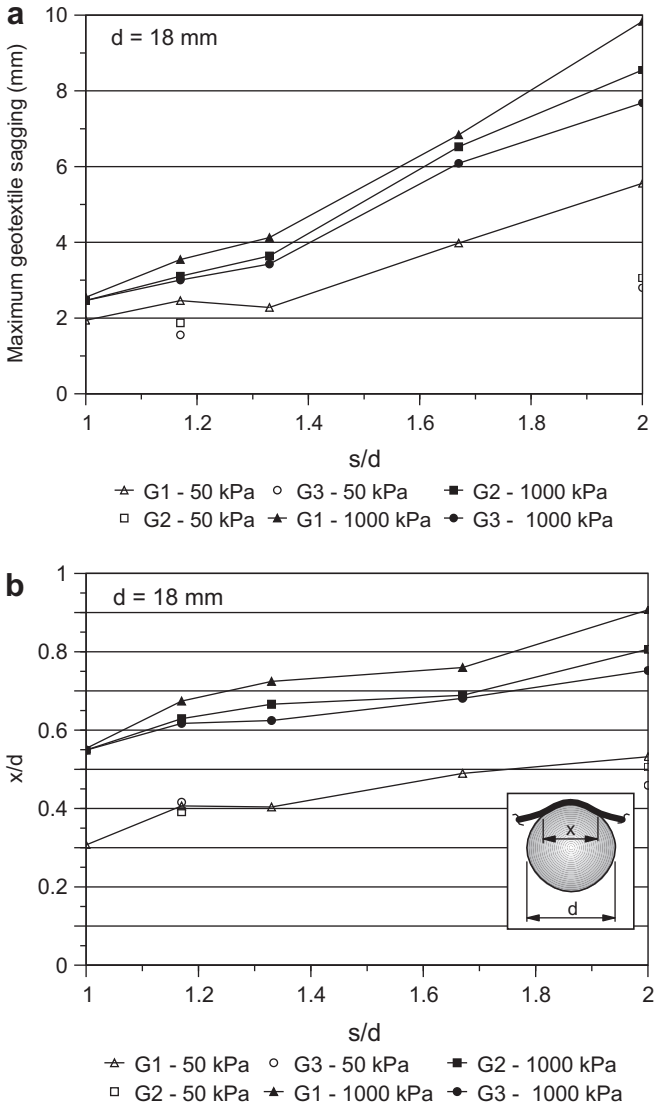

Fig. 9. Influence of geotextile mass per unit area on maximum sagging and contact area diameter. (a) Maximum sagging versus s/d. (b) x/d versus s/d.

Where: ε = average geotextile strain, δ = maximum geotextile vertical deflection in the void and b = void diameter.

Giroud et al. (1990) also provide the following equation to estimate the vertical stress acting on the geotextile (Fig. 4a) for a soil with a friction angle greater than 20°, based on works on arching theories by Terzaghi (1943) and Kezdi (1975)

$$\sigma = \gamma b\left(1 - e^{-\frac{H}{b}}\right) + \sigma_v e^{-\frac{H}{b}} \quad (4)$$

Where σ = vertical stress on the geotextile layer (Fig. 4a), γ = soil unit weight, H = soil thickness above the void, σ_v = vertical stress on the soil surface.

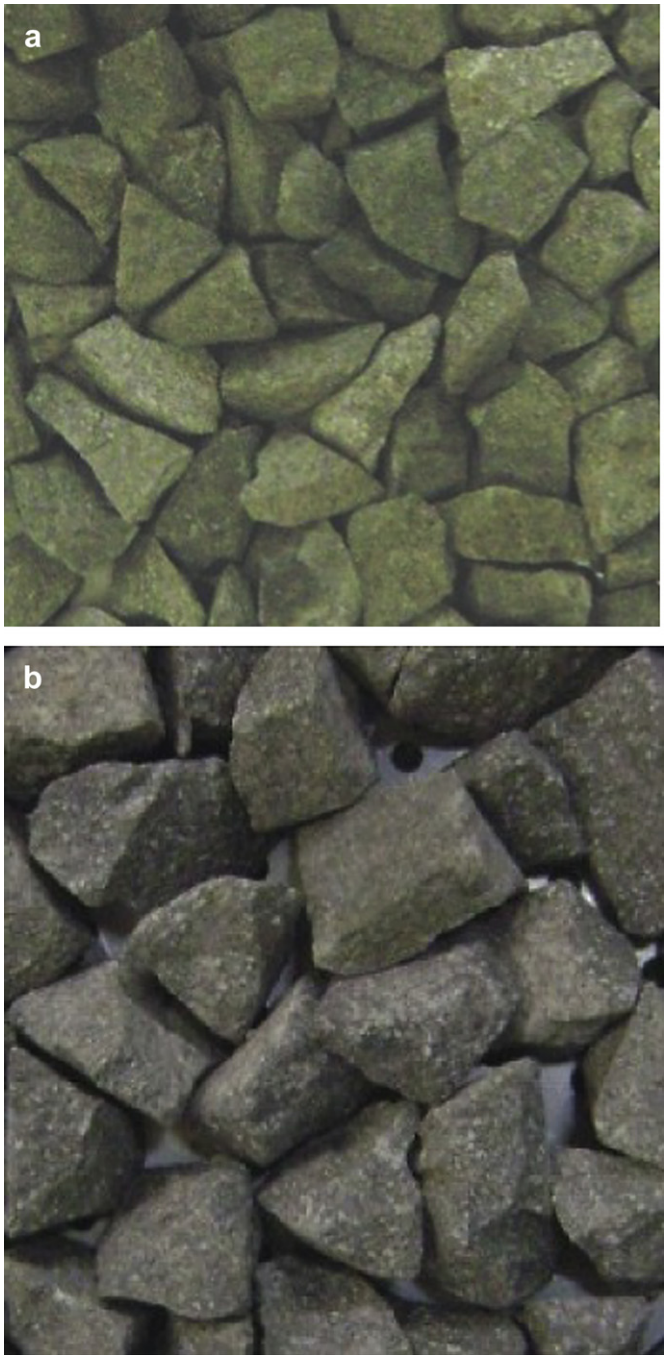

Fig. 10. Densest arrangements of gravel particles. (a) Gravel 1. (b) Gravel 3.

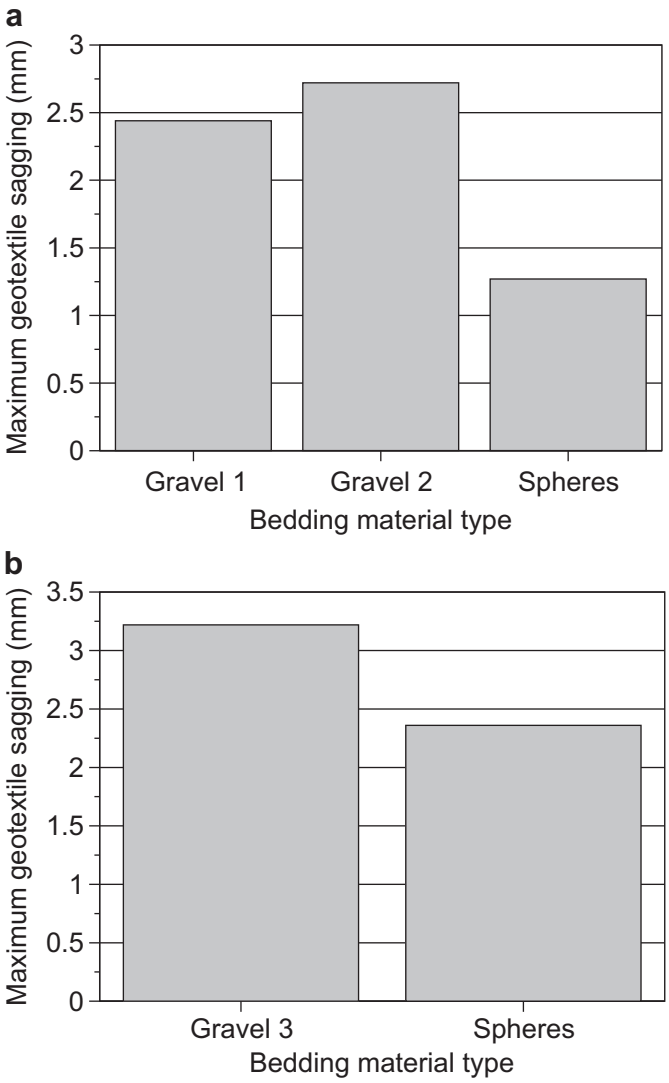

Fig. 11. Average values of maximum geotextile sagging versus particle shape and diameter – s/d = 1, geotextile G1, 500 kPa vertical stress on sample top. (a) 10 mm particle diameter. (b) 18 mm particle diameter.

As the void in between spheres in the present tests is not circular, an equivalent value for the void diameter (b_{eq}) has to be determined to use Eqs (1)–(4). The value of b_{eq} that fitted best the experimental results was equal to the diameter of the circle passing through the centre of the spheres for the triangular arrangement of spheres used in this work, which is given by

$$b_{eq} = 2s/\sqrt{3} \quad (5)$$

Fig. 15(a) and (b) show comparisons between measured and predicted average geotextile tensile strains using Eqs. (1)–(3) with

Table 3
Values of s from measurements in the pack of gravel particles.

Gravel	Average value (mm)	Standard deviation (mm)	Maximum value (mm)
1	13.5	4.1	23.9
2	12.6	4.7	30.7
3	18.8	5.6	34.4

Notes: Tests with geotextile G1 under 500 kPa normal stress.

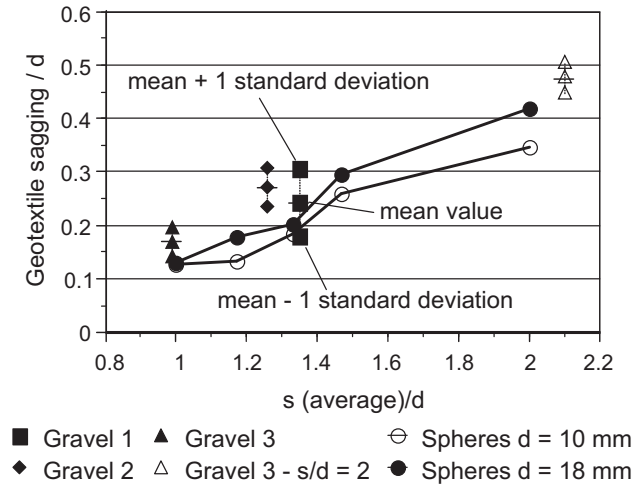

Fig. 12. Normalised geotextile sagging versus *s/d* for different bedding materials – Geotextile G1, 500 kPa.

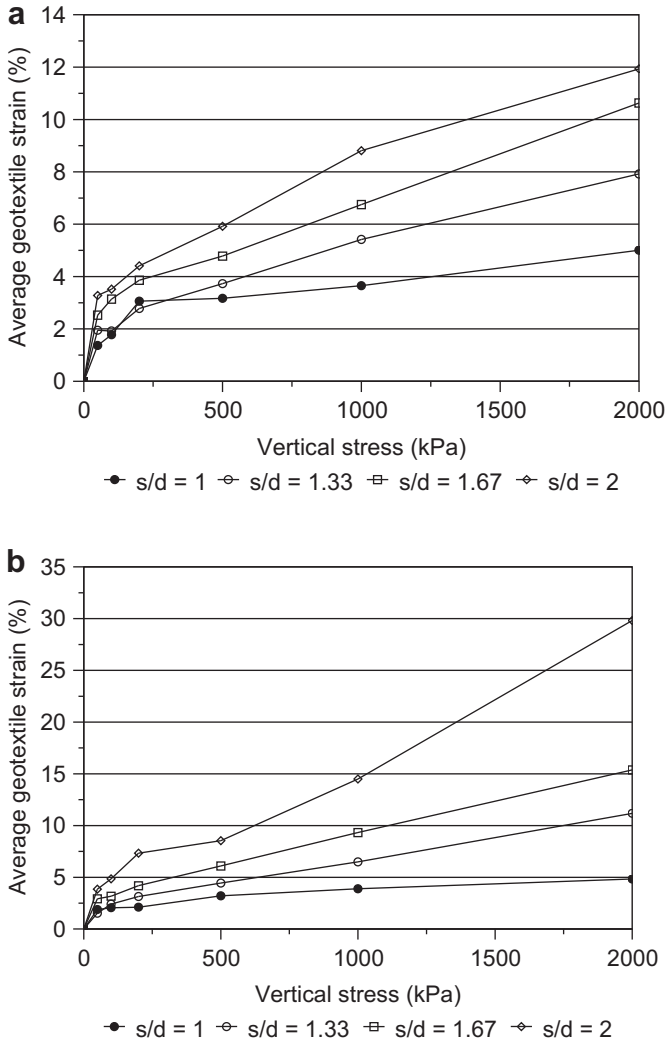

Fig. 13. Average geotextile tensile strain versus normal stress – Geotextile G1. (a) 10 mm diameter spheres. (b) 18 mm diameter spheres.

b given by Eq. (5). It can be seen that in this case predictions and measurements compared very well for the conditions employed in the testing programme reported in this paper.

It should be noted that according to Eq. (4) σ will tend to γb, for no surcharge on the soil surface and large values of H, which is a very low vertical stress for usual dimensions of voids between bedding soils particles. Therefore, the conditions of the tests and the applicability of the above equations would be more suitable for large stresses on thin layers of soils overlying the geotextile, as it may be the case during careless spreading and compaction of fills

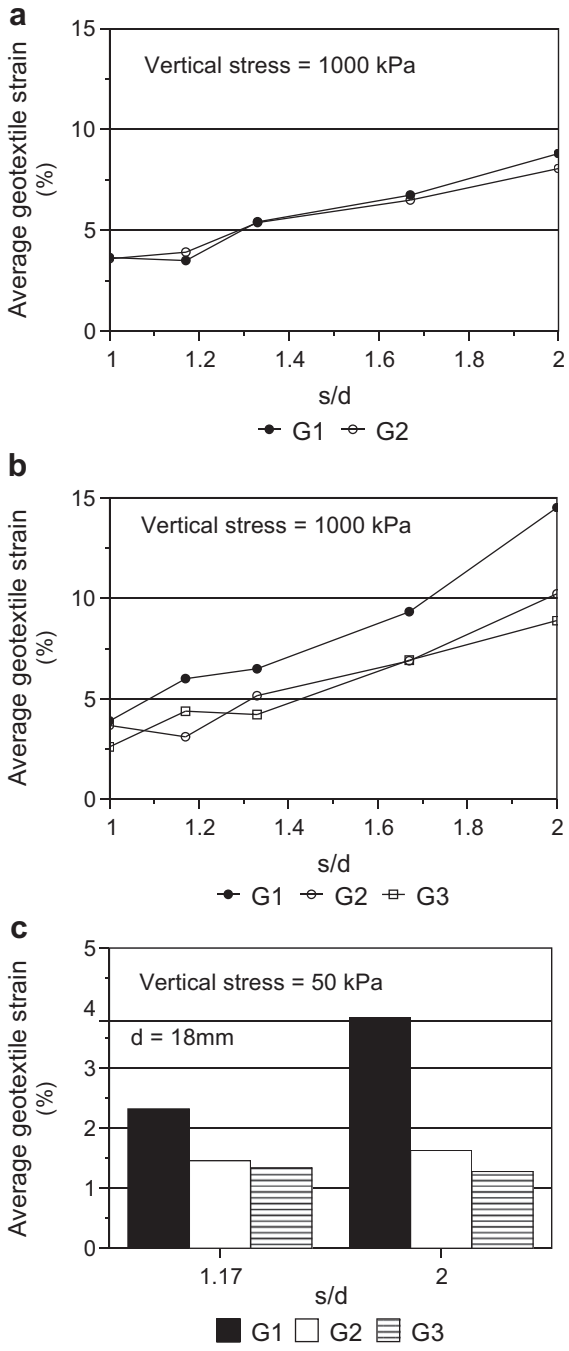

Fig. 14. Influence of geotextile mass per unit area on geotextile strains. (a) 10 mm dia. spheres – 1000 kPa vertical stress. (b) 18 mm dia. spheres – 1000 kPa vertical stress. (c) 18 mm dia. spheres – 50 kPa vertical stress.

on drainage systems incorporating geotextiles (Fig. 1) or for geotextile filters overlying boulders.

A similar exercise can be carried out to estimate average geotextile strains in packs of gravel particles, using the values of maximum geotextile sagging in between particles and the distance between the point of maximum sagging and the closest gravel particle peak (Fig. 4b and Fig. 16). Images of the deformed shape of the geotextile after the tests were employed to identify the locations of maximum sagging and to measure their distances to the closest particle peak in tests with gravels. Fig. 16 shows average geotextile strain (plus and minus one standard deviation) versus s/d for tests with gravels and geotextile G1, under 500 kPa normal stress, in a pack arrangement aiming at $s/d = 1$ and $s/d = 2$. As in the discussion of sagging in between gravel particles presented earlier in this paper, because the value of s is not uniform, average values of s were normalised by the particle diameter in the horizontal axis of Fig. 16. The results obtained in the test with spheres (for $s/d = 1$) are also plotted in this figure for comparison. The results suggest that the average geotextile strain in a pack of gravel particles can be up to 163% larger than that in a pack of spherical particles with the same diameter and spacing between particles. However, as in the case of maximum geotextile sagging versus s(average)/d (Fig. 12), the result obtained for Gravel 3 ($d = 19$ mm) with $s/d = 2$ was rather close to that of the pack of spheres with similar diameter and s/d. The results in Figs. 12 and 16 suggest that for large values of s/d the shape of the particle may be less important regarding maximum sagging and geotextile strains in between particles, bearing in mind the results obtained for spherical particles. In this case, perforation of the geotextile at the contacts with angular gravel particles is likely to be the main concern. Despite predictions using equation (1)–(5) having compared well with results of tests with spheres, the results in Fig. 16 suggest that when using those equations to estimate strains in a geotextile overlying a pack of typical gravel particles the values of geotextile strains obtained should be multiplied by a factor of the order of 3 or greater.

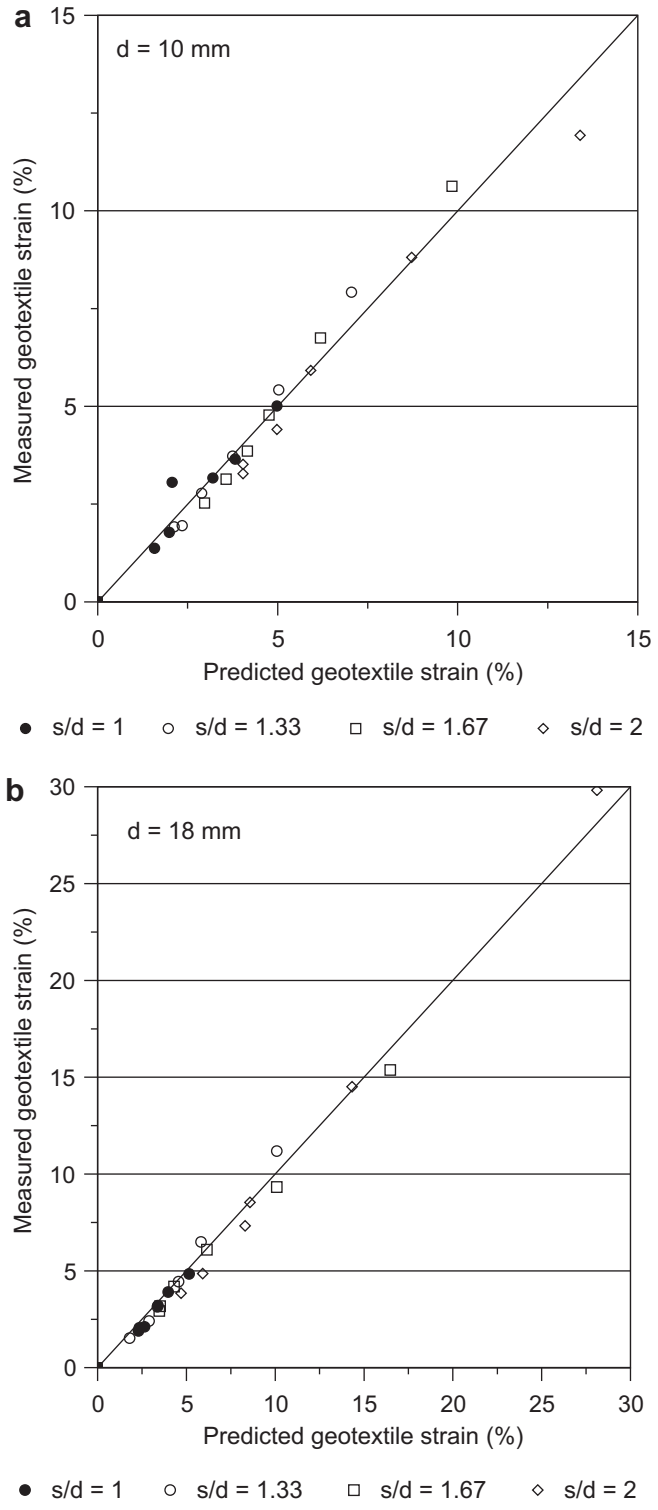

Fig. 15. Comparison between predicted and measured average geotextile strains. (a) 10 mm diameter spheres. (b) 18 mm diameter spheres.

3.4. Evaluation of geotextile retention capacity

The retention capacity of the geotextile under the deformed shape caused by the characteristics of the bedding material can be evaluated by the results in Fig. 17, for tests with a bedding material consisting of 18 mm diameter spheres. Fig. 17 presents the variation of maximum diameter (D_{95}) of the particle that piped through the geotextile filter (G1) with vertical stress on the void (σ) calculated using equation (4). Except when indicated otherwise, the piping of soil particles in these tests was caused by impacts of a rubber weight distributed along the sides of the permeameter, as previously described in this paper. In Fig. 17 the variation of the geotextile filtration opening size with normal stress obtained by Gardoni and Palmeira (2002) using bubble point tests (BBP tests) is also presented for comparison. Larger particles were capable of piping through the geotextile for lower values of normal stress and geotextile strains. This was a consequence of the influence of the presence of the holes left in the geotextile layer during the needle-punching manufacturing process. For $s/d = 1$ and a vertical stress of 2000 kPa on the soil sample top (vertical stress on the void of 181 kPa according to Eq. (4)), the piped particle diameter obtained in one of the tests was equal to 0.037 mm, which is considerably smaller than the base soil maximum particle diameter. This can be attributed to the reduced void in which the geotextile can sag in the compact sphere arrangement when s/d is equal to 1.

Fig. 17 shows that even not considering the influence of the needle holes, the size of the base soil particle capable of piping through the geotextile may be considerably larger than the geotextile filtration opening size obtained from bubble point tests. The piped particle diameter was as much as 4 times greater than the constriction diameter obtained in BBP tests when the needle hole played an important role. For vertical stresses over 20 kPa, with little or no influence of the needle holes, the piped particle diameter was up to 2 times greater than the constriction diameter obtained in BBP tests. Therefore, current retention criteria may

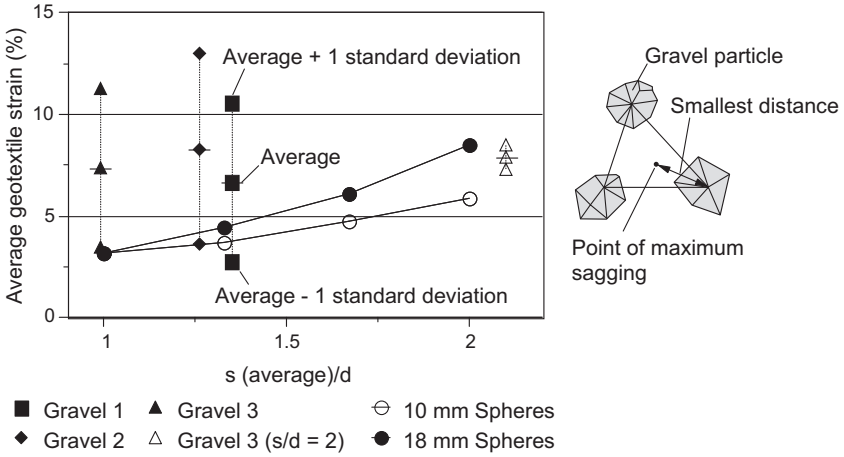

Fig. 16. Average geotextile strain versus *s/d* for different particle shapes – Geotextile G1, 500 kPa vertical stress.

overestimate the geotextile retention capacity by a factor greater than 2 in situations similar to those reported in this paper. It should be pointed out that in the bubble point tests the geotextile specimen was subjected to unidirectional compression only, due to the action of the vertical stress and that the test is not accurate enough for measurements of large openings. It should also be noted that different mechanisms (impact or water flow) for causing particle piping through the geotextile yielded similar values of D_{95} (Fig. 17).

The results obtained show that the diameter of the needle hole controls the maximum diameter of the piped particle. The needles used in the manufacturing of the geotextiles used in this study have a diameter equal to 0.7 mm. Accommodation of geotextile fibres after the needle-punching process will result in final opening diameters left by the needles smaller than that value. However, Palmeira and Fannin (1998) have observed that even under 150 kPa vertical stress (unidirectional compression) the openings left by the needles can still reach a diameter of up to 0.08 mm. For the conditions of the present tests, the way the needle hole will deform will depend on its location in the void between underlying material particles and on the state of stress around it. As the vertical stress increases, the deformation and distortion of the needle holes closest to the underlying material particles increase, also favoured by friction between base soil and geotextile. This limits the size of particles capable of passing through the geotextile or making it easier for these holes to be blocked by larger base soil particles, as schematically shown in Fig. 18(a). The worst situation is that of a hole in the central region of the void between underlying material particles. The deformed shape of the geotextile in the voids

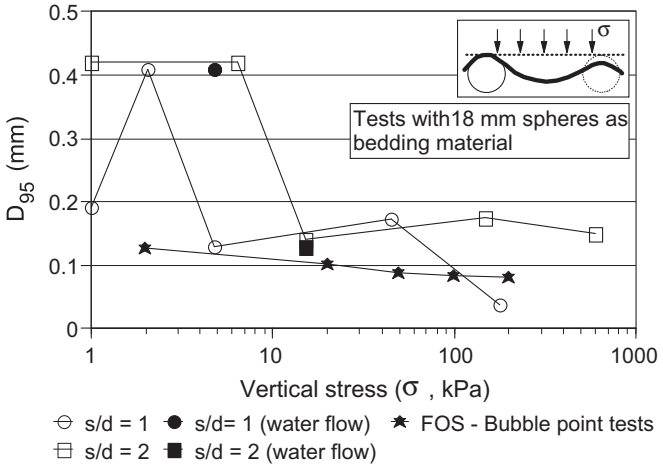

Fig. 17. Piped particle diameter versus vertical stress on the void – Geotextile G1.

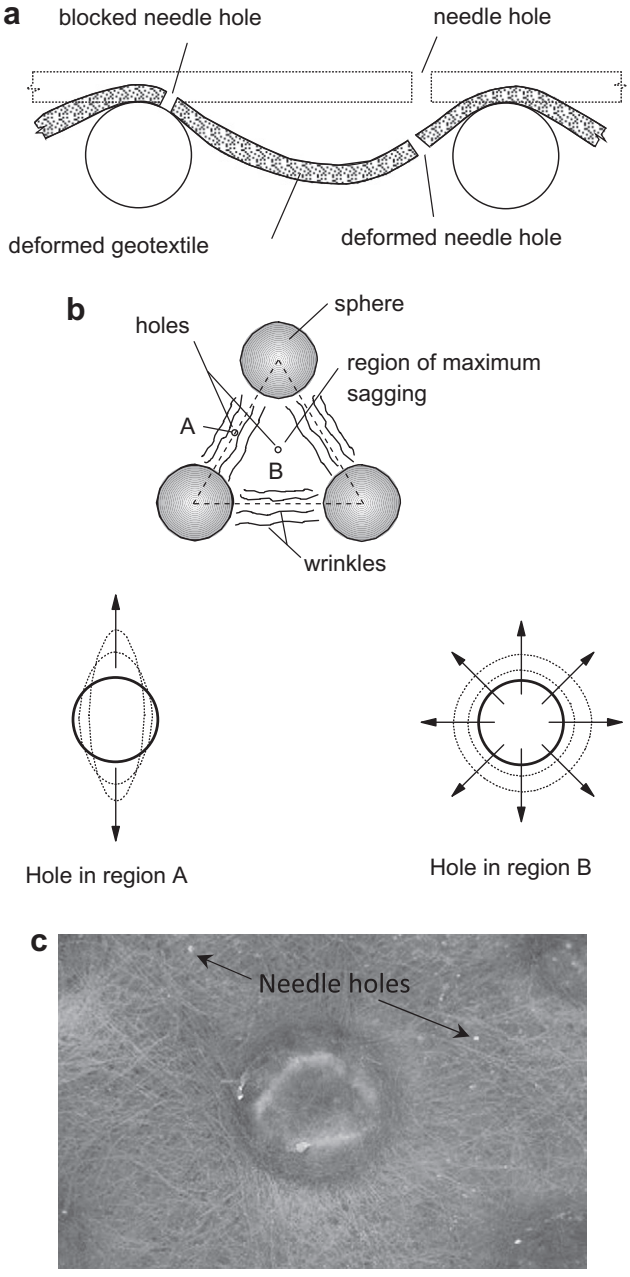

Fig. 18. Needle holes in the geotextile. (a) Distortion of holes left by needles. (b) Change of hole shape due to stretching. (c) Needle-hole in the region of maximum sagging in one of the tests.

between particles and the multi-axial state of stress around the holes in the central region of the void will tend to increase the diameter of these holes, favouring the passage of particles. For an unidirectional load an initially circular hole in a nonwoven geotextile will take an elliptical form (Mendes et al. 2007), reducing the size of the soil particle capable of passing through it, which is likely to be the case for a hole in region A in Fig. 18(b). However, for a multidirectional state of stress the diameter of the hole will tend to increase (region B in Fig. 18(b)), yielding to large soil particles being able to pipe through it. This point has been previously discussed by Fourie and Addis (1999) in filtration opening size tests on woven geotextiles subjected to tensile loads. Fig. 18(c) depicts the deformed shape of a needle hole in the region of maximum geotextile sagging in one of the tests performed, confirming that the hole left by the needle after manufacturing will provide the flow channel with largest constriction, which will control the maximum diameter of the base soil particle capable of piping through the geotextile filter.

Despite the presence of the needle holes and the large constriction sizes they provided, for the conditions of the tests reported in this paper the soil-geotextile system maintained stability during the tests, without piping failure. This was certainly due to the geotextile deformation mechanism discussed above in addition to the closure of the needle holes by large base soil particles.

4. Conclusions

This paper presented results of tests on nonwoven, needle-punched, geotextile filters overlying bedding materials consisting of spheres and gravel particles under confinement. The main conclusions obtained from the testing programme are summarised as follows:

- Maximum geotextile sagging in the voids in between bedding material particles is a function of the shape of the particles and spacing between them. For similar particle diameters and arrangements the average maximum geotextile sagging in the voids of gravel particles was up to 71% greater than that observed in test with the bedding material consisting of spheres.
- The tensile strain mobilised in the geotextile also depends on the type and spacing between particles. Average maximum strains in tests with gravels were up to 163% greater than those obtained under similar conditions in tests with spheres. The greater the geotextile mass per unit area the smaller the mobilised geotextile strain.
- The method proposed by Giroud et al. (1990) to estimate strains in geotextiles overlying voids was adapted to the conditions of the tests reported in this paper. The predictions by this method using an equivalent void diameter compared well with measurements of average strains in geotextiles overlying regular packs of spheres. However, for packs of gravel particles, the results suggest that the estimates of geotextile strains using that approach should be multiplied by a factor greater than 3.
- The holes left by the needles during the needle-punching manufacturing process may control the size of the largest base soil particle capable of piping through a needle-punched nonwoven geotextile filter. That will depend on the dimension and location of the hole with respect to the surrounding bedding soil particles. The critical situation is found when the hole is located in the region were maximum sagging occurs, because the multi-axial state of stress around the hole tends to increase its diameter, favouring the passage of larger base soil particles. Piped particle diameters as large as 2 or 4 times the constriction size obtained in bubble point tests on geotextiles subjected to unidirectional compression were observed, depending on the role played by the needle holes. That does not necessarily mean that the geotextile filter may fail in avoiding catastrophic piping failure of the base soil, as the larger soil particles may block those constrictions enlarged by geotextile stretching in the voids, depending on the base soil characteristics and the number of enlarged constrictions. Besides, geotextile impregnation by base soil particles during spreading and compaction of this soil prior to water flow may increase geotextile retention capacity. However, the retention capacity of the filter may be certainly reduced due to geotextile straining, not to mention if geotextile damage takes place in case of large voids or mechanically aggressive bedding materials. In addition, the effects of creep on the filter behaviour of a geotextile subjected to large tensile stresses cannot be ignored in long term applications. For the conditions of the tests reported in this paper the base soil-geotextile systems tested were stable, with no piping failure having been observed.
- Even when the influence of the presence of the needle holes is less important, the results obtained suggest that available retention criteria can overestimate the retention capacity of the geotextile by a factor greater than 2 in field situations similar to those simulated in the present tests. More realistic tests to evaluate the filtration opening size of geotextiles under multi-axial stresses are required for the improvement of retention criteria of geotextile overlying voids.
- The tests reported in this paper aimed to simulate the performance of nonwoven geotextile filters overlying coarse drainage materials under high vertical stresses (low soil layer thicknesses during base soil spreading and compaction, for instance) or geotextile filters overlying boulders. Due to the complexity of the problem, the results and conclusions presented in this paper should be viewed as preliminary and further research is required for a better understanding on the behaviour of geotextile filters overlying different bedding materials.

Acknowledgements

The authors are indebted to the following institutions that supported the research reported in this paper: University of Brasilia, CNPq-National Council for Scientific and Technological Development, CAPES-Brazilian Ministry of Education and FAP/DF-Federal District Foundation for Research Support.

References

Bhatia, S.K., Huang, Q., 1995. Geotextile filters for internally stable/unstable soils. Geosynthetics International 2 (3), 537–565.
Calhoun, C.C., 1972. Development of Design Criteria and Acceptance of Specifications for Plastic Filter Cloth. Technical Report S-72–77. U.S. Army Corps of Engineers, Vicksburgh, MS, USA, 83 p.
Carroll, R.G., 1983. Geotextile Filter Criteria, Transportation Research Record 916, USA, pp. 46–53.
CFGG, 1986. Normes françaises d'essais. Comité Français des Géotextiles et Géomembranes, Paris, France.
Fannin, R.J., Vaid, Y.P., Shi, Y.C., 1994. Filtration behaviour of nonwoven geotextiles. Canadian Geotechnical Journal 31, 555–563.
Faure, Y.H., Farkouh, B., Delmas, Ph., Nancey, A., 1999. Analysis of geotextile filter behaviour after 21 years in Valcros dam. Geotextiles and Geomembranes 17 (5–6), 353–370.
Fischer, G.R., Christopher, B.R., Holtz, R.D., 1990. Filter criteria based on pore size distribution. 4th International Conference on Geotextiles, Geomembranes and Related Products, The Hague, The Netherlands, vol. 1, pp. 289–294.
Fourie, A.B., Addis, P.C., 1999. Changes in filtration opening size of woven geotextiles subjected to tensile loads. Geotextiles and Geomembranes 17 (5-6), 331–340.
Fourie, A.B., Kuchena, S.M., 1995. The influence of tensile stresses on the filtration characteristics of geotextiles. Geosynthetics International 2 (2), 455–471.

Gardoni, M.G., 2000. A study on the drainage and filtration behaviour of geosynthetics under compression. PhD. Thesis, University of Brasilia, Brasilia, DF, Brazil, p. 313.
Gardoni, M.G., Palmeira, E.M., 2002. Microstructure and pore characteristics of synthetic filters under confinement. Geotechnique 52 (6), 405–418.
Giroud, J.P., 1982. Filter criteria for geotextiles. 2nd International Conference on geotextiles, Las Vegas, USA, vol. 1, pp. 103–108.
Giroud, J.P., 1996. Granular filters and geotextile filters. In: Lafleur, J., Rollin, A.L. (Eds.), GeoFilters'96. Montreal, Canada, pp. 565–680.
Giroud, J.P., Bonaparte, R., Beech, J.F., Gross, B.A., 1990. Design of soil layer-geosynthetic systems overlying voids. Geotexitles and Geomembranes 9 (1), 11–50.
Heerten, G., 1982. Dimensioning the filtration properties of geotextiles considering log-term conditions. 2nd International Conference on Geotextiles, Las Vegas, USA, vol. 1, pp. 115–120.
Kezdi, A., 1975. Lateral earth pressure. In: Winterkorn, H.F., Fang, H.Y. (Eds.), Foundation Engineering Handbook. Van Nostrand Reinhold, New York, USA, pp. 197–220.
Lafleur, J., 1999. Selection of geotextiles to filter broadly graded cohesionless soils. Geotextiles and Geomembranes 17 (5–6), 299–312.
Lawson, C., 1986. Geotextile filter criteria for tropical residual soils. In: 3rd International Conference on Geotextiles, Vienna, Austria, vol. 2, pp. 557–562.
Mendes, M.J.A., Palmeira, E.M., Matheus, E., 2007. Some factors affecting the in-soil load-strain behaviour of virgin and damaged nonwoven geotextiles. Geosynthetics International 14 (1), 39–50.
Palmeira, E.M., Beirigo, E.A., Gardoni, M.G., 2010. Tailings-nonwoven geotextile filter compatibility in mining applications. Geotextiles and Geomembranes 28 (2), 136–148.
Palmeira, E.M., Fannin, R.J., 1998. A methodology for the evaluation of geotextile pore opening sizes under confining pressure. Geosynthetics International 5 (3), 347–357.
Palmeira, E.M., Fannin, R.J., Vaid, Y.P., 1996. A study on the behaviour of soil-geotextile systems in filtration tests. Canadian Geotechnical Journal 33 (4), 899–912.
Palmeira, E.M., Fannin, R.J., 2002. Soil-geotextile compatibility in filtration. 7th International Conference on Geosynthetics, Nice, France, vol. 3, 853–872.
Palmeira, E.M., Gardoni, M.G., Bessa da Luz, D.W., 2005. Soil-geotextile filter interaction under high stress levels in the gradient ratio test. Geosynthetics International 12 (4), 162–175.
Powers, M.C., 1953. A new roundness scale for sedimentary particles. Journal of Sedimentary Petrology 23 (2), 117–119.
Terzaghi, K., 1943. Theoretical Soil Mechanics. John Wiley and Sons Inc., New York, USA.
Vaid, Y.P., Negussey, D., 1988. Preparation of Reconstituted Sand Specimens. Advanced Triaxial Testing of Soil and Rock. Special Technical Publication No. 977, American Society for Testing and Materials. 405–417.
Wu, C.-S., Hong, Y.-S., Wang, R.-H., 2008. The influence of uniaxial tensile strain on the pore size and filtration characteristics of geotextiles. Geotextiles and Geomembranes 26 (3), 250–262.
Wu, C.-S., Hong, Y.-S., Yan, Y.-W., Chang, B.-S., 2006. Soil-nonwoven geotextile filtration behavior under contact with drainage materials. Geotextiles and Geomembranes 24 (1), 1–10.